M_{max} Assessment for the Newberry EGS Demonstration at the Davenport 55-29 Site

Prepared for:

AltaRock Energy, Inc.

2320 Marinship Way, Suite 200

Sausalito, CA 94965

Prepared by:

Dean Ostenaa, Dan O'Connell, and Mark Zellman

Fugro Consultants, Inc.
William Lettis & Associates Division
1726 Cole Blvd., Suite 230
Lakewood, CO 80401

EXCUTIVE SUMMARY

The report was prepared by the William Lettis & Associates Division of Fugro Consultants, Inc. at the request of AltaRock Energy, Inc. to provide further assessment of the maximum induced earthquakes for the Newberry EGS Demonstration Project based on site-specific properties from the site.

To further evaluate maximum geologic structure length and extent which might be associated with induced earthquakes near Davenport 55-29, additional detailed analyses of LiDAR data was conducted. The objective of this evaluation was to identify the relative scales of any nearby potential faults, fractures, and features that might be present within 1 to 5 km of the well site. No significant features were disclosed within the 1-km radius of the well. Within a 5-km radius, mapped lineaments are associated with drainage and depositional features on the flanks and margins of the Newberry volcano, and are not similar to active tectonic features mapped in the broader region by Cladouhos et al., 2011.

Four alternative approaches to evaluating M_{max} for the Newberry EGS Demonstration based on physical properties of the surrounding rock mass and proposed injection process were considered. Three of these approaches provide single-valued deterministic estimates of M_{max} for specific combinations of physical parameters estimated for the site. The fourth approach provides a probabilistic estimate, but requires local knowledge of the earthquake activity rate parameters, which are less complete at Newberry.

One method (Brune, 1970) is based on dynamic stress drop, which controls the absolute amplitude of radiated seismic waves and corresponding ground shaking. The second method is based on source volume and moment (McGarr, 1976). The third method (Leonard, 2010) estimates seismic moment from fault dimensions through a scaled set of relations. The plausible range of M_{max} estimates derived from these calculations span a range of magnitudes from about **M** 3 to **M** 4 (Tables 3 through 6). The largest magnitudes require assumptions with multiple combinations of maximized or end-member parameters which appear unlikely.

The fourth magnitude estimation approach (Shapiro et al., 2010) uses injected volume, critical stress based on site characteristics, and regional earthquake recurrence information to develop probabilistic estimates of M_{max}. Probability estimates for M_{max} are estimated based on the methods of Shapiro et al. (2010) and are sensitive to the input values of regional seismicity activity parameters, but are most sensitive to hydraulic diffusivity which influences the maximum volume where pore pressures can be increased in response to injection. The preferred estimates of M_{max} probabilities (Table 9) were calculated using the highest hydraulic diffusivity derived for induced seismicity (Talwani et al., 2007) and conservative parameters for the probability equations of Shapiro et al. (2010). Based on this analysis, the probability of the Newberry injection activity inducing an event with **M** > 3.0 is less than 1% over a 50-day period that would include injection and pressure dissipation. At a 95% probability, the maximum induced event has **M** less than 2.2. The median (probability = 0.5) M_{max} for the most conservative assumptions is less than **M** 1.0. The results of ongoing local seismic monitoring planned for the demonstration project should provide a basis for updated estimates of M_{max} probabilities.

TABLE OF CONTENTS

1.0 Introduction 6
2.0 Estimates of M_{max} for the Newberry EGS 7
2.1 Evaluation of Maximum Structure Length Near Davenport 55-29 7
2.1.1 Results 9
2.2 Alternative Approaches to M_{max} Estimates 9
2.2.1 Stress Drop and Source Radius Based on Brune (1970) 10
2.2.2 Injection Volume and Rigidity Based on McGarr (1976) 11
2.2.3 Fault Length and Area Based on Leonard (2010) 12
2.2.4 Seismogenic Index Approach Based on Shapiro et al. (2010) 14
3.0 Conclusions 20
4.0 References 22

LIST OF FIGURES

Figure 1 Location Map
Figure 2 Digital Elevation Model
Figure 3 Hillslope Aspect Map
Figure 4 Slope Map
Figure 5 Digital Elevation Model with Detailed and Regional Lineaments
Figure 6 Hillslope Aspect and Regional Lineaments
Figure 7 Slope Map and Regional Lineaments
Figure 8 Geology and Compiled Lineaments
Figure 9 Newberry Induced M_{max} Probability based on Shapiro et al. (2010) for b = 0.94.
Figure 10 Newberry Induced M_{max} Probability based on Shapiro et al. (2010) for b = 1.25.
Figure 11 Newberry Induced M_{max} Probability based on Shapiro et al. (2010) for b = 0.94.
Figure 12 Newberry Induced M_{max} Probability based on Shapiro et al. (2010) for b = 1.25.

LIST OF TABLES

Table 1 Summary of Rock and Physical Properties for Newberry
Table 2 Preliminary Newberry EGS Demo Project Hydroshear Design Parameters
Table 3 M_{max} Estimates Based on Brune (1970)
Table 4 M_{max} Estimates Based on McGarr (1976)
Table 5 M_{max} Estimates Based on Fault Area (Leonard, 2010)
Table 6 M_{max} Estimates Based on Fault Length (Leonard, 2010)
Table 7 C_{max} Values from Rothert and Shapiro (2007)
Table 8 Preliminary M_{max} Probability Based on Shapiro et al. (2010)
Table 9 Summary Table of Preferred M_{max} Range and Probability Estimates

1.0 INTRODUCTION

This report provides an assessment of the Maximum earthquake (M_{max}) likely to be associated with induced seismicity from the proposed Newberry EGS Demonstration at the Davenport 55-29 well. The demonstration site is located on the west flank of Newberry Volcano south of Bend, OR (Figure 1). Details of the planned program and previous studies conducted are discussed in AltaRock (2011). An assessment of the local and regional seismic hazard for the demonstration project was completed by Wong et al. (2011). Cladouhos et al. (2011) evaluated evidence of recent faulting in the region based on newly acquired LiDAR data.

The report was prepared by the William Lettis & Associates Division of Fugro Consultants, Inc. at the request of AltaRock Energy, Inc. under P.O. ARE 002-9-0057, dated April 12, 2011. The objective is to provide further assessment of the maximum induced earthquakes for the Newberry EGS Demonstration Project based on site-specific properties from the site. Physical parameters for the Newberry Project where provided by AltaRock (Tables 1 and 2; AltaRock, 2011) along with additional information on heat flow data from the site. Recently acquired LiDAR data was provided for the evaluation by AltaRock as well.

2.0 ESTIMATES OF M_{MAX} FOR THE NEWBERRY EGS

2.1 Evaluation of Maximum Structure Length Near Davenport 55-29

The extent and orientation of potential tectonic structures in the vicinity of the injection site is an important component in the evaluation of potential M_{max} for induced earthquakes. Based on previous fault compilations (Figure 1), seismic hazard studies for the Newberry EGS project (Wong et al., 2011), as well as further evaluation of active faults by AltaRock (Cladouhos et al 2011), most elements of the active major regional fault systems do not appear to extend closer than about 20 km of the injection site, although some features which are primarily volcanic in origin extend within about 7 km of the site. Evaluation of these regional faults by Cladouhos et al. (2011) further suggests a strong concentration of active fault orientations with approximately north-south strikes. These strikes are very consistent with preliminary orientations of S_{min} based on borehole televiewer results from Davenport 55-29 (AltaRock, 2011) and are most likely orientations of structures along which induced seismicity may occur.

To further evaluate maximum geologic structure length which might be associated with induced earthquakes near Davenport 55-29, we conducted additional detailed analyses of LiDAR data provided by AltaRock Energy. The objective of this evaluation was to identify the relative scales of any nearby potential faults, fractures, and features that might be present in the well vicinity. The emphasis of this evaluation focused on features within 1 to 5 km of the well site. The analysis consisted of identification and mapping of lineaments on a variety of map bases at both large and small scales. These lineaments were then evaluated and classified on geologic and geomorphic criteria. The results provide an indication of the relative scale of geologic structure which might be considered in the evaluation for maximum induced earthquakes.

Bare-earth Light Detection and Ranging (LiDAR) digital elevation models (DEMs) and hillshade images were provided to WLA by Altarock. The LiDAR is compiled from 4 separate datasets (Area 1, 2, 3, and 11) collected by Watershed Sciences, Inc for the Oregon Department of Geology and Mineral Industries (DOGAMI). The data was collected between October 2, 2009 and July 3, 2010 at an average native density of ≥ 8 points per square meter. These raster datasets were provided in north, south, and west segments and with a 3 foot grid cell resolution.

The DEMs and associated hillshade images were the primary source of base images used for the lineament mapping (Figure 2). The north and south DEMs were merged into a single eastern segment and processed using ArcGIS 3D analyst into derivative hillslope aspect and slope (degree) maps which provided secondary and tertiary base maps for lineament mapping and analysis.

Linear features were initially mapped on the DEM hillshade image (Figure 2), as shapefile lines using ArcGIS Desktop version 10, at screen scales of 1:5,000 to 1:10,000 for the 5-km study area and slightly larger surrounding region. The mapped lineaments were then compared to the derivative maps (Figures 3 and 4), and additional linear features identified and compiled. The linear features mapped on all images are generally short segments less than 0.5 km long, with the longest segment measuring 2.5 kilometers. The mapped features were classified based on geomorphic interpretations derived from the base maps and noted in an attribute table. For each feature only one description is provided, but in some cases multiple geomorphic descriptions could be possible. The compiled and classified lineaments, along with regional lineaments discussed below, are shown on Figure 5.

Lineaments were also mapped at a large scale (1:100,000) from the DEM hillshade base (Figure 2), aspect base (Figure 3) and slope map base (Figure 4) with a new shapefile created for each map base. Features were mapped to a distance of 8 - 10 kilometers from the site. Attributes were not provided for the lineaments mapped at this scale because in many cases lineaments were composed of multiple features (stream segment, base of hill slope, benched slope, etc). These line segments are longer than those mapped from the DEM at smaller scales and reach up to 15 kilometers in length. The regional lineaments are shown on Figures 5, 6, and 7.

The final step in the lineament evaluation was to overlay the mapped lineaments on a local geologic base map (Ma et al., 2009) to assess any correlation of mapped lineaments and geology (Figure 8).

2.1.1 Results

The two compilation maps (Figures 5 and 8) best depict the aggregate patterns of mapped features near Davenport 55-29. Within a 1 km radius of the well, there is a notable lack of mapped lineaments at both detailed and regional scales. The detailed mapping lineaments within the 5 km radius are dominantly short features associated with the younger volcanic flow units north of the well. South of the well, within the 5-km radius, the detailed lineaments are dominantly erosional and drainage related. Orientations of these lineaments typically follow local slope direction. The regional scale lineament patterns are dominated by WNW-striking features in the western portion of the map and by WSW-striking features in the eastern half of the map. These features also appear to reflect primarily drainage and depositional patterns on the west flank of the Newberry Volcano, but represent a more aggregated view of smaller scale individual features. Particularly in the eastern portion of the map, the pattern of the regional lineaments appears to be associated with the constructional topography of younger volcanic units north and south of the main crater and with ring fractures of the main caldera (Figure 8).

The general patterns and characteristics of the mapped lineaments on Figures 5 and 8 do not fit the patterns of active tectonic structures mapped by Cladouhos et al (2011) on the LiDAR data over a broader region near Newberry. The active tectonic features mostly had strikes of N10°± 10° (Cladouhos et al., 2011). The lineaments mapped on Figures 5 and 8 generally have westerly strikes. An exception is a group of lineaments striking about N5°E which lie west and south of the 1-km radius, and are mapped from the regional images. These lineaments appear to coincide with erosional contacts of mapped geologic units on the west flank of Newberry (Figure 8). They are not expressed as scarps or fissures in the detailed mapping, and thus do not appear to represent evidence of a through-going structure in that area.

2.2 Alternative Approaches to M_{max} Estimates

We consider four alternative approaches to evaluating M_{max} for the Newberry EGS Demonstration based on physical properties of the surrounding rock mass and proposed injection process. Three of these approaches provide single-valued deterministic estimates of M_{max} for specific combinations of physical parameters estimated for the site. The fourth

approach provides a probabilistic estimate, but requires local knowledge of the earthquake activity rate parameters, which are less complete at Newberry.

One method (Brune, 1970) is based on dynamic stress drop, which controls the absolute amplitude of radiated seismic waves and corresponding ground shaking (Archuleta and Hartzell, 1981; Aki, 1983; Boore, 1983). The second method is based on source volume and moment (McGarr, 1976). The third method (Leonard, 2010) is based on a displacement-fault dimension (time-independent) definition of "static" stress drop, which has no first-order relationship with dynamic stress drop; dynamic stress drops determine ground shaking levels (Archuleta and Hartzell, 1981; Aki, 1983; Boore, 1983). A wide range of dynamic stress drops and rise times (the time required for full displacement to occur at each point on the fault) can produce the same "static" stress drop. The fourth magnitude estimation approach (Shapiro et al., 2010) uses injected volume, critical stress based on site characteristics, and regional earthquake recurrence information to develop probabilistic estimates of Mmax.

2.2.1 Stress Drop and Source Radius Based on Brune (1970)

Estimates of seismic moment from induced events can be calculated from stress drop and source radius using Brune (1970). Seismic moment is then converted to magnitude using the standard equations for conversion to moment magnitude (Equation 1).

$$\mathbf{M} = 2/3 \log_{10} (M_o) - 10.7 \qquad (1)$$

For this evaluation we use a range of stress drop from 1 to 3 MPa, the typical range for shallow-focus normal-faulting earthquakes (Mohammadioun and Serva, 2001). For comparison, stress drops for induced earthquakes at the Fenton Hill geothermal site ranged as high as 2 MPa and averaged <1 MPa (Fehler and Phillips, 1991). Mayeda and Walter (1996) estimated stress drops in the western United States using regional coda envelopes with corrections for attenuation. Their mean dynamic stress drop for Basin and Range earthquakes was 3.0 MPa (30 bars). Spudich et al., (1999) suggest that stress drop of 3.0 MPa (30 bars) is a reasonable stress drop for an extensional environment based on their analyses of extensional earthquake ground motion data. Ichinose et al. (1997) found stress drops of ~ 6.0 MPa (60 bars) for a normal-faulting earthquake sequence near Reno, Nevada, that contained a M 4.5 mainshock.

Doser (1986) estimated stress drops of 6-7 MPa (60-70 bars) for the three M > 6 normal-faulting earthquakes in the Fairview Peak-Dixie Valley, Nevada, earthquake sequence. Boatwright (1985) estimated dynamic stress drops 3.3 ±1.6 MPa (33 ±16 bars) and 7.7 ±5.2 MPa (77 ±52 bars) for aftershocks from two segment of the 1983 M 7.0 Borah Peak, Idaho, earthquake.

Compared to the Newberry EGS well, all the tectonic earthquakes occurred at substantially greater depths, where the maximum stress is vertical and determined by an overburden of at least 10 km thickness. Doser and Smith (1989) found that in the extensional region of the western United States that all M ≥ 7.0 earthquakes occurred at depths of ≥ 12 km. In contrast, the maximum earthquake depth associated with induced seismicity will be < 3.5 km and the maximum (vertical) stress will be about one third of the maximum stress of tectonic normal-faulting earthquakes evaluated in Boatwright (1985). Doser (1986), Mayeda and Walter (1996), Ichinose et al. (1997), Mohammadioun and Serva (2001) find that none of the normal-faulting earthquakes at depths of 7 km had dynamic stress drops > 3 MPa (30 bars). Consequently, we expect that maximum stress drop will be less than the mean dynamic stress drop of 3.0 MPa (30 bars) for Basin and Range normal-faulting earthquakes reported by Mayeda and Walter (1996), on the order of 1-1.5 MPa (10-15 bars) based on Mohammadioun and Serva (2001). However, we report a range of 1 to 3 MPa for the purposes of sensitivity testing.

Source radius is taken as 250 and 500 m, with 500 m corresponding to the expected maximum extent of the injected area as outlined by AltaRock (Table 2). As shown in Table 3, maximum magnitudes are all < **M** 4. The most plausible range of corresponds to dynamic stress drops comparable to the Fenton Hill geothermal site and shallow western U.S. extensional environments on the order of 2 MPa (20 bars) or less gives stress-drop based M_{max} in the range of **M** 3.5 to 3.8.

2.2.2 Injection Volume and Rigidity Based on McGarr (1976)

McGarr (1976) proposed a relation between seismic moment and the volume change introduced by the total injection volume. Because this approach ascribes all volume change to a single event, it may be viewed as conservative. The relation also depends on crustal rigidity, which may vary at the Newberry site (Table 1). Table 4 shows calculated M_{max} values from **M** 3.12 to

M 3.28 based on the McGarr (1976) approach using a conservative range of crustal rigidity values appropriate for the Newberry site.

2.2.3 Fault Length and Area Based on Leonard (2010)

Leonard (2010) provides an updated suite of equations which describe self-consistent scaling relations between seismic moment and fault rupture area, length, and other parameters. A subset of these relations is applicable to the relatively small fault rupture areas and lengths that are likely to be associated with EGS induced events. Seismic moment is then converted to magnitude using the standard equations for conversion to moment magnitude (Equation 1). Evaluation of the LiDAR data, and existing geologic mapping with the 5-km radius near Davenport 55-29, does not reveal the existence of significant and continuous geologic structures near the well (Section 2.1) which would exceed the length of AltaRock's proposed stimulation region of about 1 km (AltaRock, 2011). Thus, for evaluation of M_{max} based on fault length and area parameters we derive length and fault area parameters which reflect the proposed limits of the stimulation region.

The proposed development plan would create an EGS reservoir with a long dimension of 1000 m (AltaRock, 2011) or source radius of 500 m (Table 2). This value is taken as a potential strike length for the maximum faulting extent. Likewise, the vertical extent of open-hole injection (1073 m from Table 2) provides an indication of the depth extent of possible faulting. In an extensional environment, fractures and faults are unlikely to be vertical, as shown by observations of 50° dipping fractures in Davenport 55-29 (AltaRock, 2011). Thus, potential rupture areas are calculated using dips of 50° to 70° to reflect observed fracture orientations, and some tendency to develop a steeper orientation along the extent of the open hole injection. Vertical limits on fault extent beyond the open hole are also limited. The upper extent of faulting would be limited by the AltaRock injection plan to not extend above 6000 feet depth (~2 km depth; ~150 m above open hole extent). Below the open hole (~3.1 km depth), proprietary temperature data from the well suggests that a depth limit for seismogenic faulting is likely not more than about 3.5 km; at these temperatures quartz-rich rocks begin to deform by ductile flow in laboratory experiments (see, for instance, Brace and Kohlstedt, 1980) at strain rates of about 10^{-14}sec^{-1} or lower. The seismic–aseismic boundary has been used as a surrogate for the brittle-ductile transition in the crust and has been shown to correlate with the temperatures at depth of 3.5 km at Newberry in

several other studies of western U.S. crustal structure in high heat-flow regions (Gilpin and Lee, 1978; Maja and McEvilly, 1979; Sibson, 1982; and Smith and Bruhn, 1984). Thus, some additional vertical extent to the fault areas, perhaps in the range of 200 to 400 m is possible, but is limited to a maximum of about 1500 m by operational limits and the depth limit of seismogenic faulting. These larger fault extents are calculated as well to provide a bounding set of values for fault area.

The Leonard (2010) relations are probably valid for hypocentral depths > 5 km, but application to depths < 3.5 km is highly uncertain and may not be valid. Stress drops of shallow-focus (< 3.5 km depth) normal-faulting earthquakes are systematically smaller than for deeper crustal earthquakes (Mohammadioun and Serva, 2001). Both the empirical normal-faulting earthquake data (Mohammadioun and Serva, 2001) and laboratory modeling of the strength of the crust versus depth for different slip-type regimes (Scholz, 1990) indicate that it is most appropriate to consider a stress-drop for depths < 3.5 km that is half the stress drop for depths of larger-magnitude normal-faulting earthquakes. We consider 1.5 MPa as representative of the likely mean stress drop for < 3 .5 km normal-faulting events and 3.0 MPa as representative of deeper, tectonic normal-faulting events, consistent with Mohammadioun and Serva (2001) and Mayeda and Walter (1996), as discussed in Section 2.2.1. In the Leonard (2010) formulation, scaling is proportional to a constant stress drop, thus, this constant is reduced by 0.5 to correspond to the stress drop reduction from 3.0 MPa to 1.5 MPa for shallow earthquakes. This reduces log M_o estimates from Leonard (2010) by about 0.3 log units relative to the standard Leonard (2010) estimates. Estimates for “shallow” and “deep” earthquakes are tabulated separately in Tables 5 and 6 to represent expected M_{max} values.

Tables 5 and 6 summarize the ranges of calculated values for M_{max} based on potential fault extent inferred from the AltaRock injection plans (Table 2 and AltaRock, 2011). For shallow stress drop estimates, M_{max} values based on fault area and fault length for the injection depth and possible maximum depth of induced seismicity depth range from about **M** 3.7 to **M** < 4. Larger M_{max} values require combined assumptions of high stress drop, low fault dip, and significant extension of the fault area in the vertical dimensions above and below the open hole injection section.

2.2.4 Seismogenic Index Approach Based on Shapiro et al. (2010)

Shapiro et al. (2010) analyzed injection-seismicity data from six geothermal and hydrocarbon reservoirs and found that there is a time-invariant site-specific seismogenic index that might have useful predictive value for estimating the largest induced magnitude associated with an entire injection program. The Shapiro et al. (2010) analysis is appealing because it provides a probabilistic prediction of maximum magnitude based on a relatively modest amount of site-specific information. Unfortunately, it requires a parameter that is not known a-priori, the tectonic potential, which could be estimated after a relatively short duration of injection, depending on the system response. Since the tectonic potential is not known a-priori for Newberry, we start with the Shapiro et al. (2010) analysis of the Paradox Valley injection well and seismicity response to evaluate strategies to boot-strap estimates of tectonic potential prior to acquiring site-specific Newberry injection-seismicity measurements.

We present the Shapiro et al. (2010) approach starting with their magnitude predictive equations and work back to the assumptions and derivation of the equation. Analysis of the Paradox Valley injection-seismicity data illustrates a strategy to make an initial estimate of tectonic potential based on planned injection and site parameters.

Based on the reasonable assumption that induced seismicity occurrence will exhibit Poisson behavior, Shapiro et al. (2010) compute occurrence probability of *n* events with magnitude larger than **M** in a specified time interval for the important case of the probability ($P(0,\mathbf{M},t)$) of the absence of an event with a magnitude larger than a given **M** in the time interval from the start to the end of injection.

$$P(0,\mathbf{M},t) = exp(-Qc(t)10^{\Sigma - b\mathbf{M}}) \quad (2)$$

Qc(t) is the cumulative injected volume at the time at the end of injection, *b* is the slope of the cumulative magnitude-recurrence for the site, Σ is their seismogenic index,

$$\Sigma = a - \log(F_t S) \quad (3)$$

F_t is the "tectonic potential" from Shapiro et al. (2007) and S is the poroelastic uniaxial storage coefficient, which is relatively well constrained to the range of S=10^{-6} m^{-1} $\pm$ 0.5 10^{-7} for limestone and Newberry intrusive rocks (Domenico and Schwartz, 1997). The actual value of a used in Shapiro et al. (2010) to predict Mmax, depends of the potential volume of perturbed crust and the duration that the pore-pressure perturbation exists in that volume. Since a is usually reported from earthquake recurrence calculations in units of 1/(km^2*year), it is necessary to determine the seismogenic thickness appropriate for the region to convert a to units of 1/(km^3*year). Then the duration that pore-pressure perturbations will remain elevated during and after injection must be determined along with the depth range and lateral extent of the pore-pressure perturbation. With this information (duration and perturbed pore-pressure volume), a can be normalized (multiplied by volume and time) to yield the nondimensional a required for application in Shapiro et al. (2010). A conservative approach to estimate the volume, is to use the maximum hydraulic diffusivity associated with induced seismicity of 10 m^2/s from Talwani et al. (2007) to calculate the fracture extent over the duration of elevated pore pressure, and thus maximum lateral extent of the pore-pressure perturbation; this maximizes the nondimensional estimate of a.

The tectonic potential has the advantage of only depending on the tectonic activity of the injection region, but depends on a critical maximum pressure parameter, C_{max}, and the concentration of pre-existing cracks N,

$$F_t = C_{max} / N \tag{4}$$

Rothert and Shapiro (2007) developed the concept of critical pressure, C, which is the pore pressure necessary to create displacement along a crack. For a network of random pre-existing cracks, Rothert and Shapiro (2007) indicates that in the first approximation C is uniformly distributed between its minimal and maximal values, C_{min} and C_{max}, with values on the order of 10^2 to 10^6 Pa., respectively. C_{max} is usually larger than the injection caused pressure perturbation (excluding maybe a small volume around the source). Rothert and Shapiro (2007) estimate C_{max} from induced seismicity at their sites (Table 7). Nominally, the ratio of C_{max} to the applied overpressure in Table 2 is the ratio of minimum effective stress to maximum effective stress from Pine and Batchelor (1984), SR, given by

$$SR=(1+\sin\phi)/(1-\sin\phi) \quad (5)$$

where ϕ is the friction angle.

Although Rothert and Shapiro (2007), Shapiro et al. (2007), Shapiro and Dinske (2009), and Shapiro et al. (2010) never document the units they use for *a* in Equation (3), Cladouhous (pers. comm., 2011) inquired and found that *a* was considered nondimensional in these publications. Thus, appropriate use and specification of *a* is based on the unit volume of potentially induced seismicity and the duration that pore pressures remain elevated in response to injection, to yield a simple probability distribution for M_{max}. We illustrate how appropriate scaling of *a* works using injection and induced seismicity from the Paradox Valley injection well where the initial injection lasted 14 days, a total volume of 11,000 m^3, and fluid at injected overpressures1.5-4 times higher (33 MPa, Ake et al., 2005) than the proposed Newberry 8-24 MPa injection overpressure range (Table 2). We then evaluate the Shapiro et al. (2010) prediction for the four year-period at Paradox Valley leading up to the observed M_{max} at Paradox Valley of 4.3.

Shapiro et al. (2010) estimate Σ =-2.5 from the first 9 days of an unspecified injection period at Paradox Valley. We calculate C_{max} using the eight years of injection spanned by the analyses of Shapiro et al. (2007). The effective radius of injection pressure induced seismicity for this period is about 2 km (Denlinger et al., 2010), into a formation thickness of 200 m (Bremkamp and Harr, 1988), which is a small fraction of the depth range of the seismogenic crust for the region of about 15 km (Ake et al., 2005). This formation thickness is much less than the depth span of the perforated zones because the perforations below the Leadville formation were quickly sealed by precipitates. We adjust the *a* estimate of -1.795 from LaForge (1997) for the 8-year time period and the volume of potential activity (2 km radius over 200 m thickness) to obtain a nondimensional estimate of *a* of -1.67. We use information from Paradox Valley on friction angle (40 degrees from Bremkamp and Harr (1988), $S=10^{-6}$ m^{-1}, and fracture density of 0.5 (Bremkamp and Harr, 1988), the duration of injection considered by Shapiro et al. (2010) of eight years, and the Paradox Valley Σ=-2.5 from Shapiro et al. (2010) to back-calculate C_{max} for Paradox Valley (Table 7). The estimated Paradox Valley C_{max} of 16 MPa is close to the well-

head fluid injection pressure of ~17 MPa associated with the onset of induced seismicity (Ake et al., 2005).

To check the consistency of the estimated C_{max} of 16 MPa for Paradox Valley and the M_{max} prediction approach of Shapiro et al. (2010), we calculate the M_{max} for the initial 1991 14-day injection sequence that injected a total volume of 11,000 m^3. We calculate M_{max} for a period of 30 days to correspond to the time initially required for pressure to decline after injection was stopped (Ake et al., 2005). During this initial injection the perforated active injection sections extended from the top of the Leadville at about 4.2 km depth into basement at 5.1 km. Consequently, we use a formation thickness of 1 km for the initial injection sequence. We use a hydraulic diffusivity of 10 m^2/s, calculated using well measurements of permeability in the fractures from initial injection well test (Bremkamp and Harr, 1988), to establish the radius of the potentially affected area around the well. We use the initial injection period *b*-value from Ake et al. (2005) *b*=0.82 to calculate the M_{max} probability for the initial 1991 Paradox Injection sequence (Figure 9). The observed M_{max}=0.9 falls within the 95% confidence region of M_{max} < 1.2 (Figure 9). This suggests that using a reasonable estimate of C_{max} and the region recurrence information appropriately scaled for the injection characteristics (volume and time), yields a reasonable estimate of M_{max} for the total volume injected using a sufficient time for the pressure to decrease after injection stops.

We also calculated M_{max} for the 1996-2000 period at Paradox Valley where injection rates were held at their highest values. This period of induced seismicity culminated with the occurrence of a **M**=4.3 earthquake in May 2000 (Ake et al., 2005), the largest induced Paradox Valley earthquake to date that represents the observed M_{max} at Paradox Valley. For this case we use a formation thickness of 200 m because the lower perforations were sealed by precipitate and a time period of 4 years to rescale *a* from LaForge (1997) along with the C_{max} of 16 MPa in (2) and (3) to estimate M_{max} probability (Figure 10). The observed Paradox Valley M_{max}=4.3 is close to the median prediction of M_{max} =4.39 (Figure 10). This result is probably not directly applicable to a closed loop geothermal system, because a total net volume of > $2*10^6$ m^3 of fluid were injected at high pressure at Paradox Valley over four years, so this result may be of more interest for sequestration activities than EGS activities. However, it does suggest that the Shapiro et al. (2010) approach may be useful for injection storage applications.

We have applied Shapiro et al. (2010) to estimate probabilistic maximum magnitude for the maximum injected volume scenario (30,545 m^3 in Table 2). We consider two approaches to apply Shapiro et al. (2010). Both approaches scales *a* to the volume surrounding the well that would be subject to increased pressures in a 50 day time period to allow for pressure decline after injection ceases. The first approach uses the maximum hydraulic diffusivity associated with induced seismicity of 10 m^2/s from Talwani et al. (2007); they determined that hydraulic diffusivity values of fractures associated with seismicity are between 0.1 and 10 m^2/s. Hydraulic diffusivities > 10 m^2/s are associated with aseismicity based on Talwani et al.'s (2007) analysis of more than 90 case histories of induced seismicity and cases of aseismicity in response to injection and reservoir impoundment. This large hydraulic diffusivity produces the most conservative estimate of M_{max} that could be associated with induced seismicity. The second approach uses the hydraulic diffusivity expected at the site of 0.2 m^2/s (Table 1), which is still in the range of hydraulic diffusivities (0.1-10 m^2/s) associated with induced seismicity from injection and reservoir impoundment (Talwani et al., 2007).

Based on testing results for sample Granite N2 4281 2H provided by AltaRock, we conservatively used the largest observed ratio of overpressure to C_{max} from Table 2 to correspond to a friction angle of 20°, a crack density of 0.5/m, S=5*10^{-7} m^{-1} from Table 1, and the Southern Cascade *a*=-2.11 km^2/year and *b*=0.94 estimate from Wong et al. (2010) in equations (2) through (5) to estimate the maximum induced magnitude (Figure 11 and Table 8). This calculation suggests that the probability of an induced event associated with the planned Newberry injection activity with **M** > 3.0 is < 1% and a 95% probability the maximum induced event has **M** < 2.2. The median maximum magnitude for the most conservative assumptions is less than **M**=1.0.

To illustrate the sensitivity to recurrence parameters and hydraulic diffusivity, the calculations were performed using Southern Cascade recurrence parameters and the Northern Basin and Range source zone recurrence parameters of Wong et al. (2010) as shown in Figures 11 and 12 and Tables 8. These calculations show a much stronger sensitivity to hydraulic diffusivity than *a*- or b-value, indicating the importance of seismic monitoring in response to initial injection to characterize effective seismic hydraulic diffusivity for the site vicinity. These results also

indicate that use of activity rates or site parameters from other potentially analogous geothermal or volcanic regions with higher background tectonic activity rates such as Coso or Long Valley (Wong et al., 2011) will not provide any more meaningful estimates of the M_{max} probability for the Newberry site.

The a-priori application of Shapiro et al. (2010) is somewhat speculative, but we have used multiple conservative assumptions on C_{max}, and the maximum possible volume affected by pore-pressure perturbation using the maximum hydraulic diffusivity associated with induced seismicity. Consequently, we suggest that the range of M_{max} in Table 8 from Shapiro et al. (2010) represents the most realistic a-prior estimate of M_{max}, particularly in light of the apparent M_{max} predictive capabilities of Shapiro et al. (2010) for the short initial 14-day injection sequence at the Paradox Valley injection well (Figure 9) as well as the 4-year long-term large-storage-volume injection that induced a **M** 4.3 earthquake (Figure 10). However, the most appropriate application of the Shapiro et al. (2010) approach would be to calculate the seismogenic index, Σ, from the first several days of injection and update the estimate of maximum magnitude based on actual site responses to early injection. Since Shapiro et al. (2010) demonstrate that the seismogenic index is time invariant, early estimation of Σ from injection activities would provide a more realistic and robust estimate of maximum induced magnitude than any a-priori approach. This updated empirical site-specific maximum induced magnitude estimate would be valuable to evaluate how to operate the injection to meet project objectives.

3.0 CONCLUSIONS

Additional lineament analyses of LiDAR data did not disclose any significant features within the 1-km radius of the well. Within a 5-km radius, mapped lineaments are associated with drainage and depositional features on the flanks and margins of the Newberry volcano, and are not similar to active tectonic features mapped in the broader region by Cladouhos et al., 2011.

Estimates of M_{max} are derived by three approaches (stress drop based on Brune, 1970; injection volume and rigidity based on McGarr, 1976; fault parameter based on Leonard, 2010) from ranges of physical dimensions of proposed demonstration process and Newberry-specific properties of the surrounding rocks. The plausible range of M_{max} estimates derived from these calculations span a range of magnitudes from about **M** 3 to **M** 4 (Tables 3 through 6). The largest magnitudes require assumptions with multiple combinations of maximized or end-member parameters which appear unlikely.

Available data indicate that normal-faulting earthquakes tend to have smaller dynamic stress drops than reverse-faulting earthquakes (Mohammadioun and Serva, 2001). This result is consistent with dynamic rupture simulations that show smaller dynamic stress drops and longer rise times during normal-faulting rupture (Brune, 1996; Shi et al., 1998; Oglesby et al., 1998; 2000; O'Connell et al., 2007). Thus, for the same moment magnitude, normal-faulting earthquakes have lower ground motions than strike-slip and reverse-slip earthquakes, as found in empirical analyses strong ground motions (Spudich et al., 1999; Pankow and Pechman, 2004, 2006; Abrahamson and Silva, 2008; Boore and Atkinson, 2008; Campbell and Bozorgnia, 2008; and Chiou and Youngs, 2008). In particular, the new ground motion prediction equations developed and released as part of the Next Generation Attenuation (NGA) Project sponsored by the Pacific Earthquake Engineering Research Center (PEER) Lifelines Program are generally considered “state-of the-practice” in the earthquake engineering community and all show reductions of 10-20% in normal-faulting peak velocities (Abrahamson and Silva, 2008; Boore and Atkinson, 2008; Campbell and Bozorgnia, 2008; and Chiou and Youngs, 2008), the ground shaking parameter that has the strongest association with human perception of ground shaking and impact of shaking on structures (Siskind et al., 1980). Thus, the ground shaking associated

with M_{max} will probably be lower than what is typically experienced in strike-slip and reverse-faulting environments.

Probability estimates for M_{max} are estimated based on the methods of Shapiro et al. (2010) and are sensitive to the input values of regional seismicity activity parameters, but are most sensitive to hydraulic diffusivity which influences the maximum volume where pore pressures can be increased in response to injection. The preferred estimates of M_{max} probabilities (Table 9) were calculated using the highest hydraulic diffusivity derived for induced seismicity (Talwani et al., 2007) and conservative parameters for the probability equations of Shapiro et al. (2010). Based on this analysis, the probability of the Newberry injection activity inducing an event with **M** > 3.0 is less than 1% over a 50-day period that would include injection and pressure dissipation. At a 95% probability, the maximum induced event has **M** less than 2.2. The median (probability = 0.5) M_{max} for the most conservative assumptions is less than **M** 1.0. The results of ongoing local seismic monitoring planned for the demonstration project should provide a basis for updated estimates of M_{max} probabilities.

4.0 REFERENCES

Abrahamson, N.A., and W.J. Silva (2008), Summary of the Abrahamson & Silva NGA ground-motion relations, Earthquake Spectra, v. 24, n. 1, 67-97.

Aki, K. (1983), Strong-motion seismology, in "Earthquakes: Observation, Theory, and Interpretation", H. Kanamori and E. Boschi, eds., Proc. of the Int. School of Physics., Enrico Fermi, North-Holland Pub. Co., Amsterdam, pp. 223-250.

AltaRock Energy, 2011, Hydroshearing controls and mitigation of induced seismicity at the Newberry EGS Demonstration, Internal document, 52 pp.

Archuleta, R.J., and Hartzell, S.H. (1981), Effects of fault finiteness on near-source ground motions, Bull. Seism. Soc. Am., 71, 939-957.

Boatwright, J, (1985), Characteristics of the aftershock sequence of the Borah Peak, Idaho, earthquake determined from digital recordings of the events, Bulletin of the Seismological Society of America; October 1985; v. 75; no. 5; p. 1265-1284.

Boore, D. M. (1983), Stochastic simulation of high-frequency ground motions based on seismological models of the radiated spectra, Bull. Seism. Soc. Am. 73, 1865-1894.

Boore, D.M., and G.M. Atkinson (2008), Ground-motion prediction equations for the average horizontal component of PGA, PGV, and 5% damped PSA at spectral periods between 0.01 s and 10.0 s, Earthquake Spectra, v. 24, n. 1, 99-138.

Bremkamp, W., and C. L. Harr (1988). Area of least resistance to fluid movement and pressure rise, Paradox Valley Unit, Salt Brine Injection Project, Bedrock, Colorado, a report prepared for the U.S. Bureau of Reclamation, Denver, Colorado, 39 pp.

Brune, J.N., 1970, Tectonic stress and the spectra of seismic shear waves from earthquakes, Journal of Geophysical Research, v. 75, p. 4997-5009.

Brune, J. (1996). Particle motions in a physical model of shallow angle thrust faulting, Proc. Indian Acad. Sci. (Earth Planet. Sci.), 105, L197–L206.

Campbell, K.W. and Y. Bozorgnia (2008), NGA ground motion model for the geometric mean component of PGA, PGV, PGD, and 5% damped linear elastic damped response spectra for periods ranging from 0.01 s to 10 s, Earthquake Spectra, v. 24, n. 1, 139-171.

Chiou, B. and R.R. Youngs (2008), An NGA model for the average horizontal component of peak ground motion and response spectra, Earthquake Spectra, v. 24, n. 1, 173-215.

Cladouhos, T., S. Petty, O. Callahan, W. Osborn, S. Hickman, and N. Davatzes, 2011, The Role of Stress Modeling in Stimulation Planning at the Newberry Volcano EGS Demonstration Project, PROCEEDINGS, Thirty-Sixth Workshop on Geothermal Reservoir

Engineering, Stanford University, Stanford, California, January 31-February 2, 2011, pp. 630-637.

Denlinger, R.P., Roeloffs, E., and D.R.H. O'Connell, 2010, Changes in seismicity and stress in response to fluid injection, Paradox Valley, Colorado, American Geophysical Union, Fall Meeting 2010, abstract #S13B-1999.

Domenico, P.A., and Schwartz, F.W., 1997, Physical and ChemicalHydrogeology: John Wiley & Sons, New York, 506 p.

Dorbath, L., Cuenot, N., Genter, A., and Frogneux, M., 2009, Seismic response of the fractured and faulted granite of Soultz-sous-Forêts (France) to 5 km deep massive water injections: Geophys. J. Int., v. 177, pp 653-675.

Doser, D.I., 1986, Earthquake processes in the Rainbow Mountain-Fairview Peak-Dixie Valley, Nevada, region 1954-1959, J. Geophys. Res., v. 91, p. 12,572-12,586.

Doser, D.I., and Smith, R.B., 1989, An assessment of source parameters of earthquakes in the cordillera of the western United States, Bull. Seism. Soc. Am., v. 79, p. 1383-1409.

Fehler and Phillips, 1991 Fehler, M.C. and Phillips, W.S., 1991, Simultaneous inversion for Q and source parameters of microearthquakes accompanying hydraulic fracturing in granitic rock: Bulletin of the Seismological Society of America, v. 81, p. 553-575.

Gilpin, B., and Lee, T. C., 1978, A microearthquake study of the Salton Sea geothermal area, California: Seismological Society of America Bulletin, v. 68, p. 441–450.

Ichinose, G.A., Smith, K.D., and Anderson, J.G., 1997, Source parameters of the 15 November 1995 Border Town, Nevada, earthquake sequence, Bull. Seism. Soc. Am., v. 87, p. 652-667.

LaForge, R. L., 1997. Seismic hazard assessment for Navajo Dam, Navajo Indian Irrigation Project, New Mexico: Seismotectonic Report No. 96-11, U. S. Bureau of Reclamation, Seismotectonics and Geophysics Group, Technical Service Center, Denver, Colorado, 34 p.

Leonard, 2010 Leonard, M., 2010, Earthquake fault scaling: self-consistent relating of rupture length, width, average displacement, and moment release: Bulleting of the Seismological Society of America, v. 100, p. 1971-1988.

Ma, Lina, Ian P. Madin, Keith V. Olson, Rudie J. Watzig, Ray E. Wells, Alan R. Niem, and George R. Priest (compilers), Oregon geologic data compilation [OGDC], release 5 (statewide), 2009

Maja, E. L., and McEvilly, T., 1979, Seismological investigations at the Geysers geothermal field: Geophysics, 44, p. 246–269.

Mayeda, K. and W. R. Walter, 1996, Moment, energy, stress drop, and source spectra of western United States earthquakes from regional coda envelope, J. Geophys. Res., v. 101, p. 11,195-11,208.

McGarr (1976 McGarr, A., 1976, Seismic moments and volume changes: J. Geophys. Res., v. 81, p. 1487.

Mohammadioun, B. and L. Serva, 2001, Stress drop, slip type, earthquake magnitude, and seismic hazard, Bull. Seism. So. Am., vol. 91(4), p.694-707.

O'Connell, D.R.H., S. Ma, and R.J. Archuleta, 2007, Influence of dip and velocity heterogeneity on reverse- and normal-faulting rupture dynamics and near-fault ground motions, Bull. Seis. Soc. Am., vol. 97, 1970-1989; DOI: 10.1785/0120070042.

Oglesby, D.D., R.J.Archuleta, and S. B. Nielsen, 1998, Earthquakes on dipping faults: The effects of broken symmetry, Science 280, 1055-1059.

Oglesby, D.D., R.J.Archuleta, and S. B. Nielsen, 2000, The three-dimensional dynamics of dipping faults, Bull. Seism. Soc. Am. 90, 616 - 628.

Pankow, K.L., and J.C. Pechmann, 2004, The SEA99 ground motion predictive relations for extensional tectonic regimes: Revisions and a new peak ground velocity relation, Bull. Seism. Soc. Am. 94, 341-348.

Pankow, K.L., and J.C. Pechmann, 2006, Erratum: The SEA99 ground motion predictive relations for extensional tectonic regimes: Revisions and a new peak ground velocity relation, Bull. Seism. Soc. Am. 96, 364.

Pine, R. and A. Batchelor, 1984, Downward imgration of shearing in jointed rock during hydraulic injections, Int. J. Rock Mechanics Mining Sciences and Geomechanical Abstracts, 21, 249-263.

Rothert, E. and S. A. Shapiro, 2007, Statistics of fracture strength and fl uid-induced microseismicity, J. Geophys. Res., 112, B04, 309, doi: 10.1029/2005JB003,959.

Scholz, C. H., 1990, The Mechanics of Earthquakes and Faulting, Cambridge University Press, New York, 439 pp.

Shapiro, S. A., and C. Dinske (2009). Scaling of seismicity induced by nonlinear fluid-rock interaction, J. Geophys. Res.,114, B09307, doi:10.1029/2008JB006145.

Shapiro, S.A., Dinske, C., and Kummerow, J., 2007, Probability of a given-magnitude earthquake induced by a fluid injection: Geophysical Research Letters, v. 34, p. L22314.

Shapiro, S.A., Dinske, C., Langebruch, C., and Wenzel, F., 2010, Seismogenic index and magnitude probability of earthquakes induced during reservoir fluid stimulations: The Leading Edge, Special Section: Microseismic, p. 304-309.

Shi, B., A. Anooshehpoor, J. N. Brune, and Y. Zeng, 1998, Dynamics of thrust faulting: 2D lattice model, Bull. Seism. Soc. Am., 88, 1484–1494.

Sibson, R. H., 1982, Fault zone models, heat flow, and depth distribution of seismicity in the continental crust of the United States: Seismological Society of America Bulletin, 72, 151–163.

Siskind, D.E., Stagg, M.S., Kopp, J.W., and Dowding, C.H., 1980, ‘‘Structural Response and Damage Produced by Ground Vibration from Blasting,’’: Report of Investigation No. 8507, United States Bureau of Mines.

Smith, R. B., and Bruhn, R. L., 1984, Intraplate extensional tectonics of the eastern Basin-Range: Inferences on structural style from seismic reflection data, regional tectonics, and thermal-mechanical models of brittle-ductile deformation: Journal of Geophysical Research, 89, 5733–5762.

Spudich, P., Joyner, W.B., Lindh, A.G., Boore, D.M., Margaris, B.M., and Fletcher, J.B., 1999, SEA99: A revised ground motion prediction relation for use in extensional tectonic regimes, Bull. Seism. Soc. Am., v. 89, p. 1156-1170.

Talwani, P., L. Chen, and K. Gahalaut (2007), Seismogenic permeability, k_s, J. Geophys. Res., 112, B07309, doi:10.1029/2006JB004665.

U.S. Geological Survey and New Mexico Bureau of Mines and Mineral Resources, 2006, Quaternary fault and fold database for the United States, accessed March, 2011, from USGS web site: http//earthquake.usgs.gov/regional/qfaults/.

Weldon, R. J., Fletcher, D. K., Weldon, E. M., Scharer, K. M., and McCrory, P. A., 2002, An update of Quaternary faults of central and eastern Oregon, *U.S. Geological Survey Open-File Report* 02-301, 26 map sheets, scale 1:100,000, 1 CD-ROM.

Wong et al 2011 Wong, I., S. Pezzopane, M. Dober, and F. Terra, 2010, Evaluation of Induced Seismicity / Seismic Hazards and Risk, for the Newberry Volcano EGS Demonstration, internal report to AltaRock Energy, 24 November 2010.

Table 1. Summary of Rock and Physical Properties for Newberry (T. Cladouhos, pers. Comm., 2011)

Input parameter	Symbol	Value (SI Units)	Value (oilfield units)
Friction angle[1]	ϕ	20°-45°	20°-45°
McGarr constant	K	~1.0	~1.0
Rock rigidity	μ	2.0->3.0 GPa	290,000->435,000 psi
Young's Modulus	E	5.0 GPa	725,000 psi
Poisson's ratio	ν	0.22	0.22
Hydraulic diffusivity	D	0.2 m^2/s	2 x10^{11} D/s
Dynamic viscosity	η	0.0001 Pa.S	0.1 cP
Permeability	K	10^{-17} m^2	0.01 mD
Porosity	ψ	0.02	0.02
Crack density from TAMU	ε	0.5	0.15

Table 2. Preliminary Newberry EGS Demo Project Hydroshear Design Parameters (T. Cladouhos, pers. Comm., 2011)

Input parameter	Symbol	Value (SI Units)	Value (oilfield units)
Well head Pressure	WHP	8.3 -> 24.1 MPa	1200-3500
Open hole fluid pressure @ shoe-6450 ft	P	26-42 MPa	3800->6100 psi
Open hole fluid pressure @ mid -8255 ft	P	31-47 MPa	4500->6800 psi
Open hole fluid pressure @ TD -10060 ft	P	36-52 MPa	5200->7500 psi
Volume per stimulation	V	19090->30545 m^3	5.0->8.0 Mgal
Peak Rate	Q	32-50 l/s (1.9-3.0 m^3/min)	500-800 gpm
Duration per stimulation	t	7days	7days
Stimulation dimension	R	500 m	1640 ft
Well diameter		21.6 cm	8.5 inch
Open hole length		1073 m	3520 ft

Table 3. M_{max} Estimates Based on Brune (1970)

Magnitude (M)	Stress Drop (MPa)	Radius (m)
3.89	3	500
3.57	1	500
3.28	3	250
2.97	1	250

Table 4. M_{max} Estimates Based on McGarr (1976)

Magnitude (M)	μ (GPa)	Injected Volume (m^3)
3.12	2	30,545
3.19	2.5	30,545
3.24	3	30,545
3.28	3.5	30,545

Table 5. M_{max} Estimates Based on Fault Area (Leonard, 2010)

Shallow Stress Drop		Deep Tectonic faults		Source Parameters			
Magnitude (M)	log M_o*	Magnitude (M)	log M_o*	Area (km^2)	Strike Extent or Length (m)	Vertical Extent (m)	Dip
3.94	15.02	4.14	15.32	1.40	1000	1073	50 °
3.89	14.94	4.09	15.24	1.24	1000	1073	60°
3.85	14.89	4.05	15.19	1.14	1000	1073	70°
4.02	15.13	4.22	15.43	1.66	1000	1073+200	50°
4.08	15.22	4.28	15.53	1.92	1000	1073+400	50°
* log M_o = (1.5 x log A) + 6.1 for A > 0 (Leonard, 2010; Table 5, dip slip faults); reduced by 0.3 for shallow							

Table 6. M_{max} Estimates Based on Fault Length (Leonard, 2010)

Shallow Stress Drop		Deep Tectonic faults		Source Parameters
Magnitude (M)	log M_o*	Magnitude (M)	log M_o*	Strike Extent or Length (m)
3.19	13.90	3.39	14.20	500
3.80	14.80	4.00	15.10	1000
* log M_o = (3 x log L) + 6.1 for L > 0 (Leonard, 2010; Table 5, dip slip fault) reduced by 0.3 for shallow				

Table 7. C_{max} Values from Rothert and Shapiro (2007)

Site	Overpressure (MPa)	C_{max} (MPa)
Fenton Hill	14	8
Soult-sous-Forêts	12	4
Cotton Valley	10	2
Paradox Valley	34	16

Table 8. Preliminary M_{max} Probability Based on Shapiro et al. (2010)

Magnitude (M)	South Cascades Source Parameters (a = -2.11, b=0.94)		Northern Basin and Range Parameters (a =-2.44, b=0.82)	
	D=10 m^2/s	D=0.2 m^2/s	D=10 m^2/s	D=0.2 m^2/s
1	4×10^{-1}	1×10^{-2}	3×10^{-1}	7×10^{-3}
2	6×10^{-2}	1×10^{-3}	5×10^{-2}	1×10^{-3}
3	8×10^{-3}	2×10^{-4}	8×10^{-3}	1×10^{-4}
4	9×10^{-4}	2×10^{-5}	1×10^{-3}	2×10^{-5}

Table 9. Summary Table of Preferred M_{max} Range and Probability Estimates

Magnitude (M)	Preliminary Probability M_{max} > M Ranges	
1	4×10^{-1}	7×10^{-3}
2	6×10^{-2}	1×10^{-3}
3	8×10^{-3}	1×10^{-4}
4	9×10^{-4}	2×10^{-5}

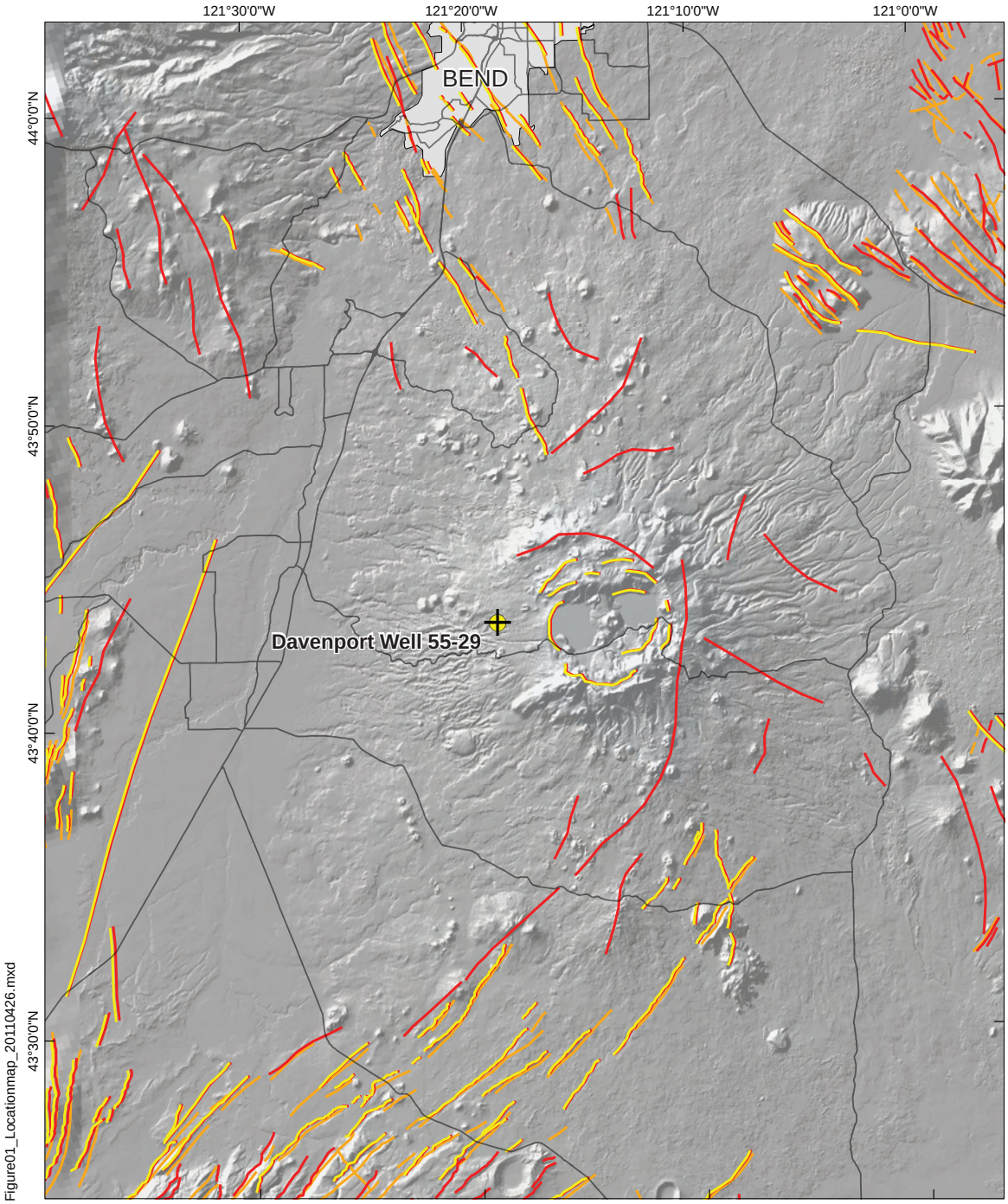

Explanation

- Fault, USGS QFF (USGS, 2011)
- Fault, OGDC-5 (Ma et al., 2009)
- Fault, Weldon et al., 2002

0 10 km
1 INCH = 10 KM

N

Location Map

FIGURE 1

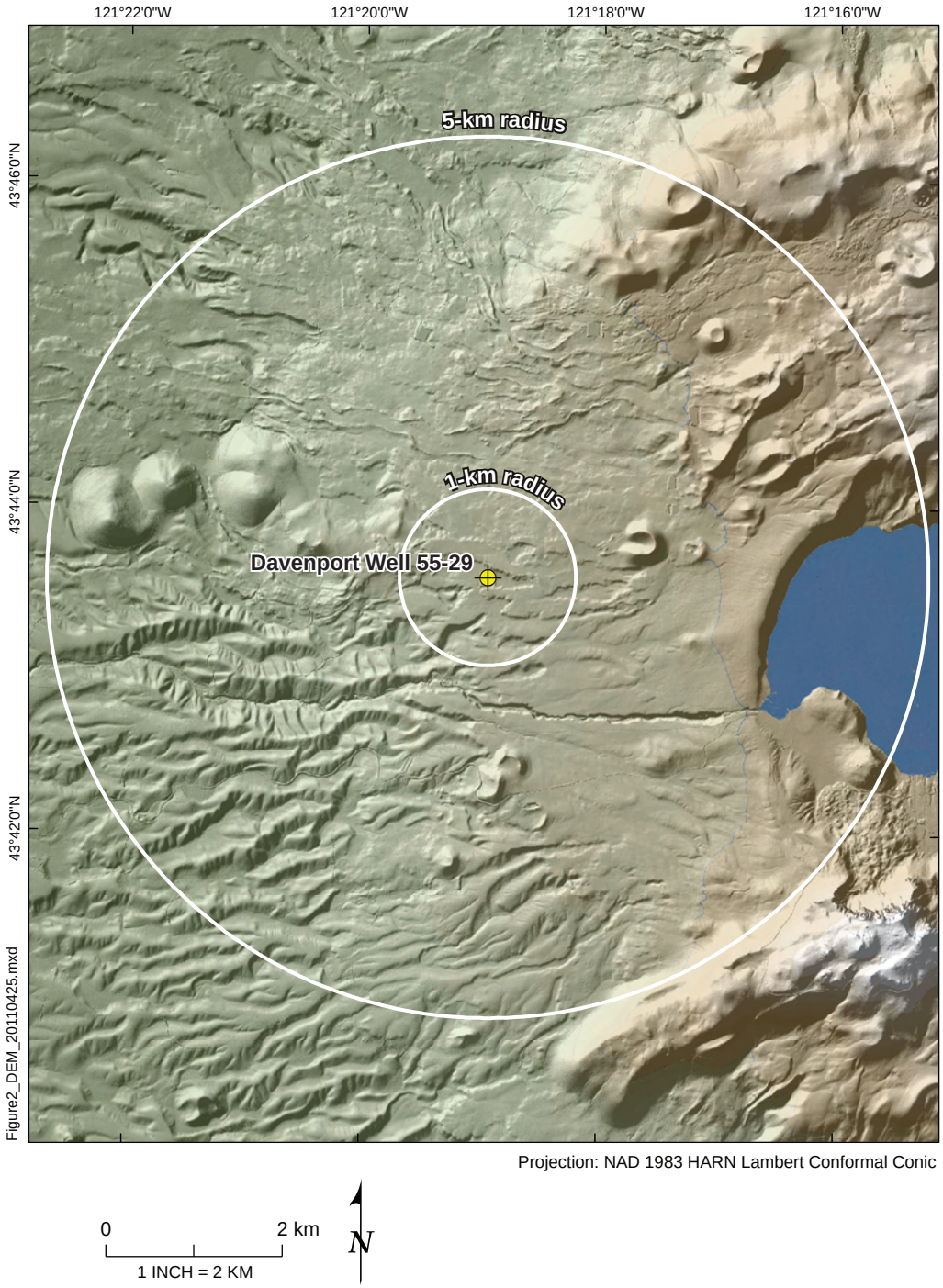

Digital Elevation Model

FIGURE 2

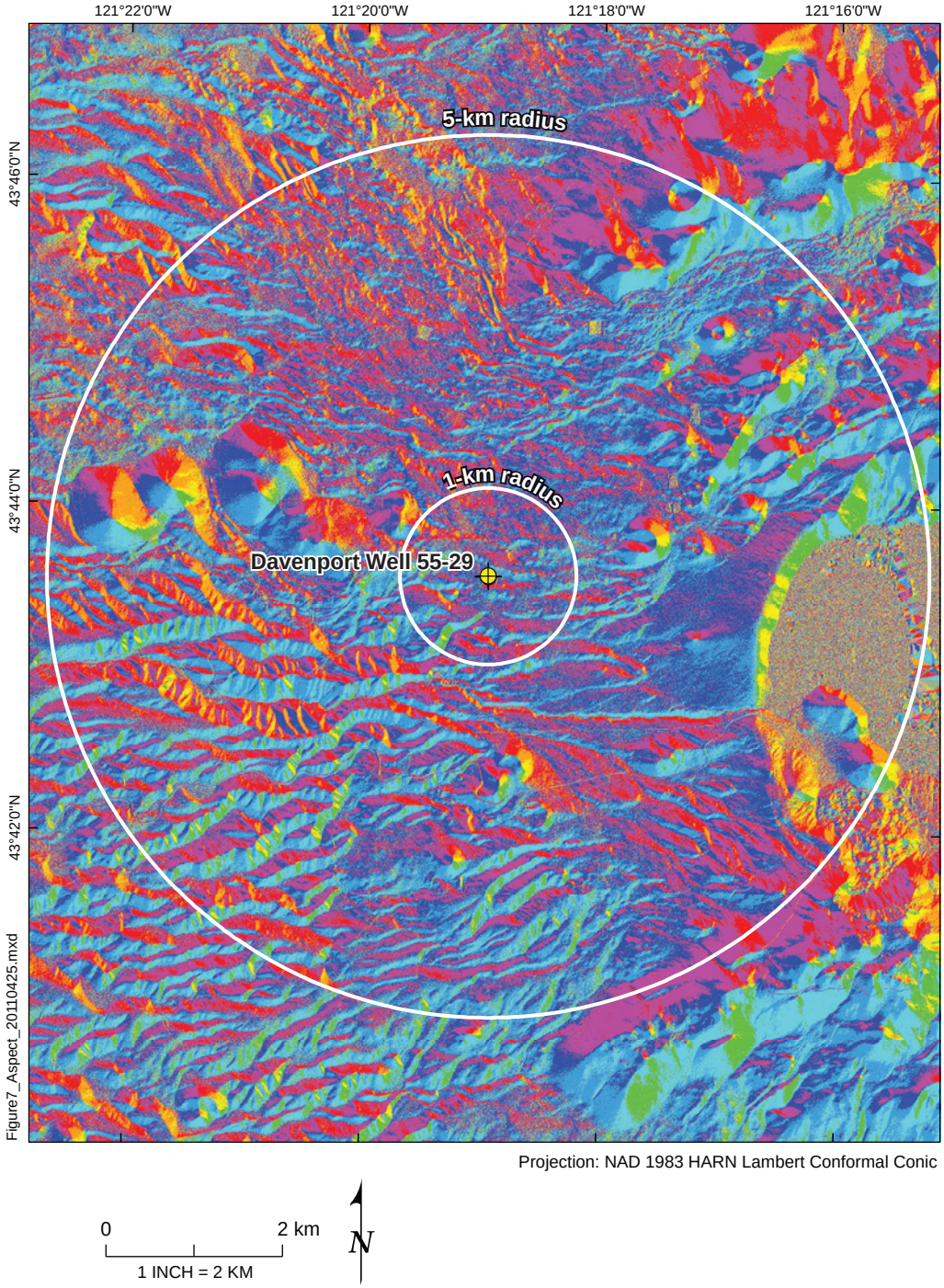

Hillslope Aspect Map

FIGURE 3

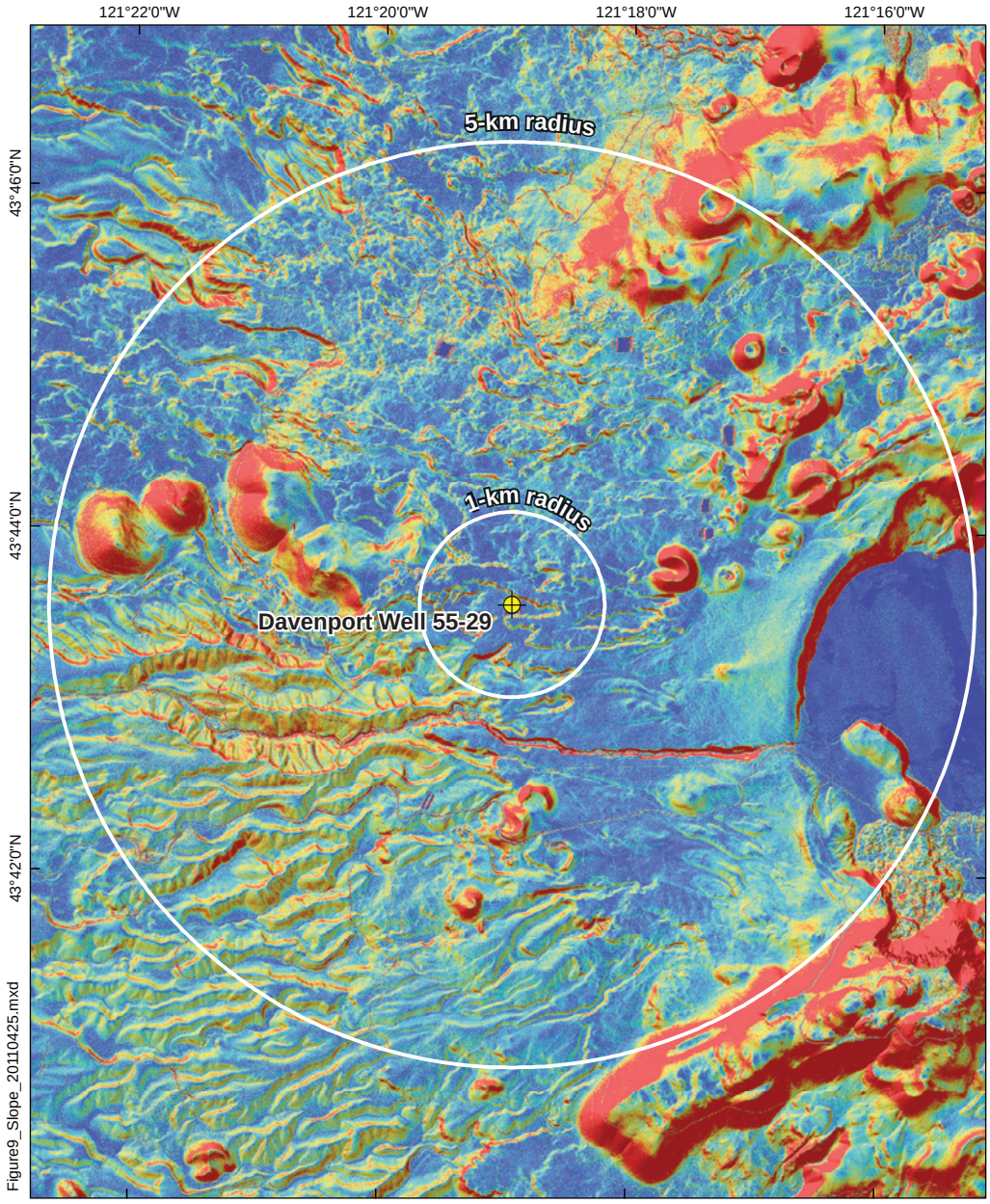

Projection: NAD 1983 HARN Lambert Conformal Conic

Explanation

Slope
High : 88.9986°
20°
Low : 0°

0 2 km
1 INCH = 2 KM

N

Slope Map

FIGURE 4

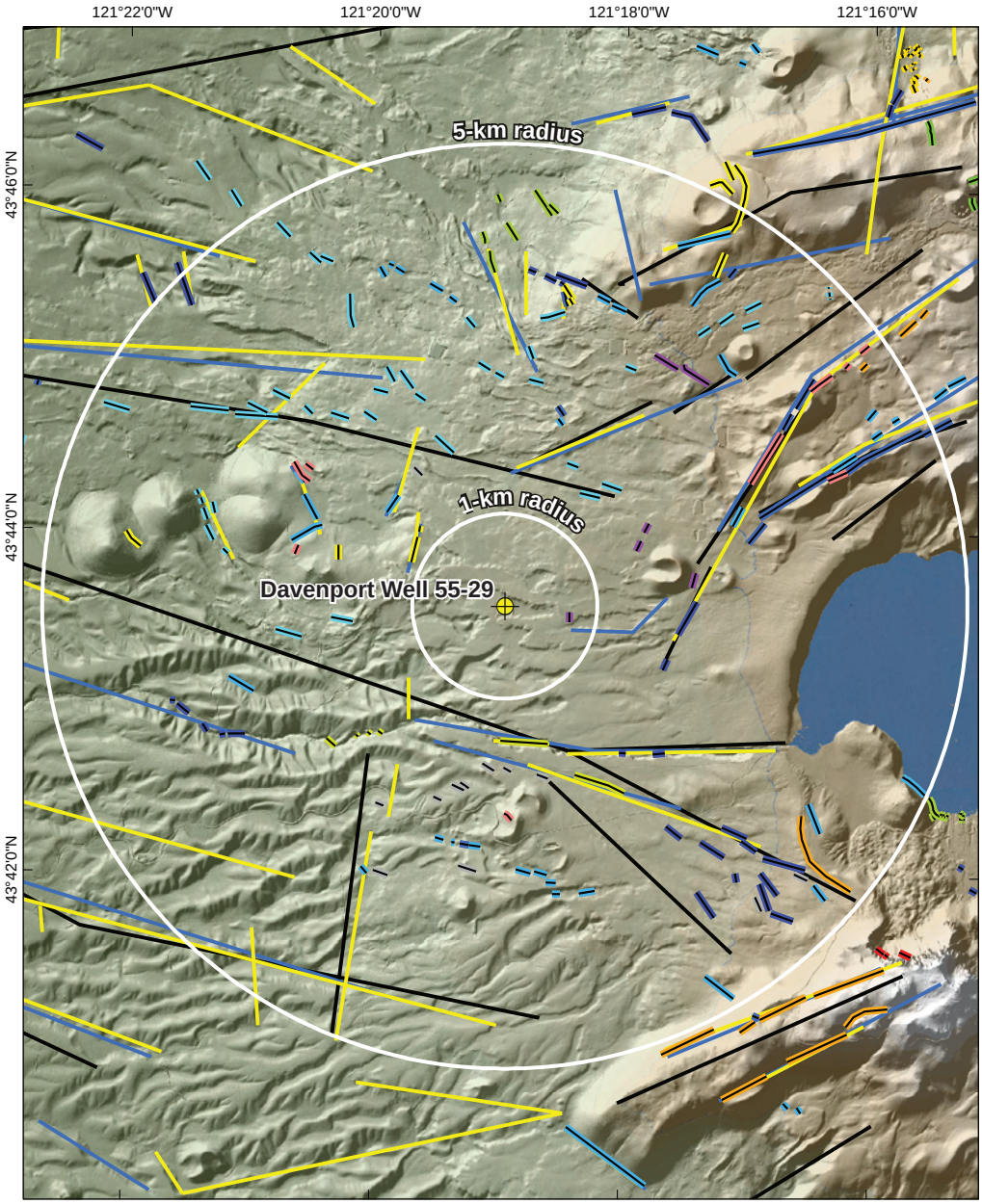

Figure4_DEM_20110425.mxd

Projection: NAD 1983 HARN Lambert Conformal Conic

Explanation

Regional lineament mapping source

- LiDAR DEM
- Slope map
- Hillslope aspect map

Detailed Mapping Lineaments

- Aligned vent
- Base of hillslope
- Erosional
- Fissure/fracture/scarp, in flow
- Flow texture
- Joint
- Linear drainage segment
- Linear ridge
- Notched terrain
- Scarp, volcanic flank
- Scarp oblique to slope
- Scarp, other
- Slope bench / break in slope
- Swale or depression

0 — 2 km
1 INCH = 2 KM

N

Digital Elevation Model with Detailed and Regional Lineaments FIGURE 5

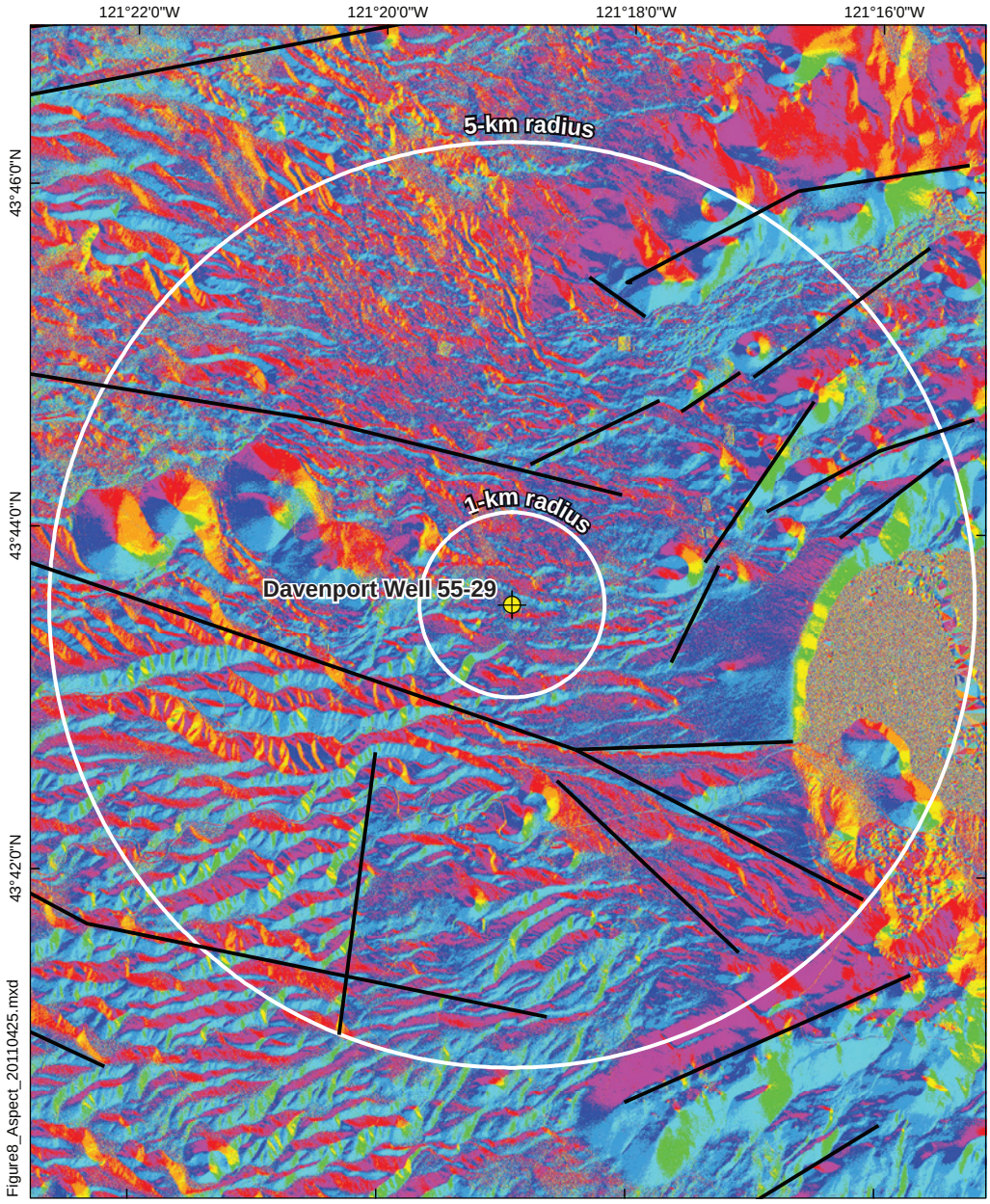

Projection: NAD 1983 HARN Lambert Conformal Conic

0 2 km
1 INCH = 2 KM
N

Hillslope Aspect and Regional Lineaments

FIGURE 6

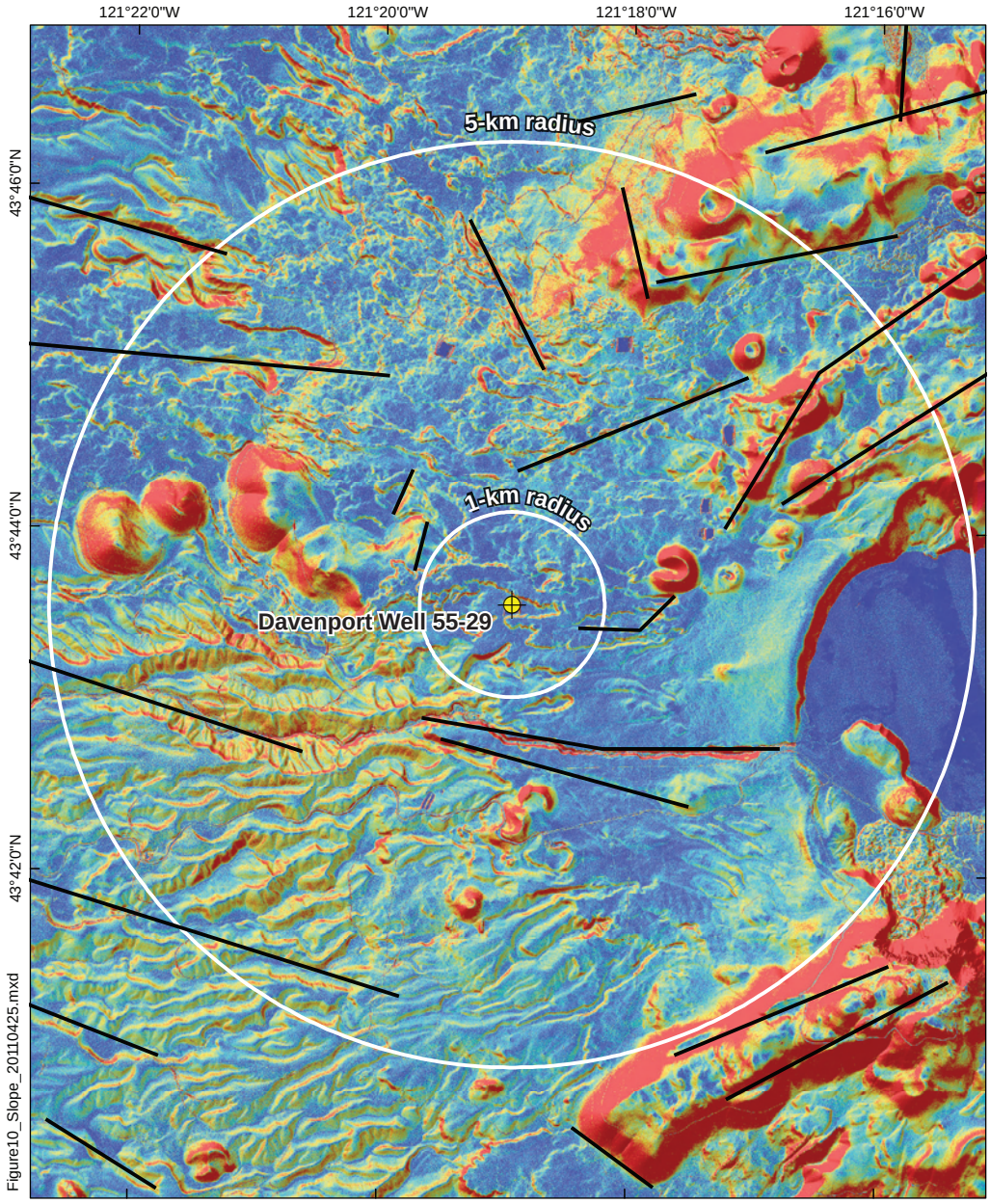

Projection: NAD 1983 HARN Lambert Conformal Conic

Explanation

Slope
High : 88.9986°
20°
Low : 0°

0 2 km
1 INCH = 2 KM

N

Slope Map and Regional Lineaments

FIGURE 7

Projection: NAD 1983 HARN Lambert Conformal Conic, Geology from Ma et al., 2009

N

0 2 km

1 INCH = 2 KM

Explanation

Geologic Units

- Qat — Andesitic tuff
- Qba — Basaltic andesite
- Qboa — Ash-flow deposits
- Qbt — Basaltic andesite lapilli tuff
- Qc — Cinder-cone and fissure-vent deposits
- Qd — Dacite dome and flows
- Qer — Early rhyolitic domes and flows
- Qgs — Gravel and sand of the caldera
- Qls — Landslide deposit
- Qrd — Rhyodacite domes and flows
- Qrpl — Rhyodacite of Paulina Lake
- Qrpp — Rhyodscite of Paulina Peak
- Qrps — Rhyodacite pumice deposits of the southwest flank
- Qsp — Sedimentary and pyroclastic deposits
- Qyb9 — Lava Cascade flow
- Qyc — Young cinder-code and fissure-vent deposits
- Qyt — Young rhyolitic tephra

Detailed Mapping Lineaments

- Aligned vent
- Base of hillslope
- Erosional
- Fissure/fracture/scarp, in flow
- Flow texture
- Joint
- Linear drainage segment
- Linear ridge
- Notched terrain
- Scarp, volcanic flank
- Scarp oblique to slope
- Scarp, other
- Slope bench / break in slope
- Swale or depression

Regional lineament mapping source

- LiDAR DEM
- Slope map
- Hillslope aspect map

Geology and Compiled Lineaments

FIGURE 8

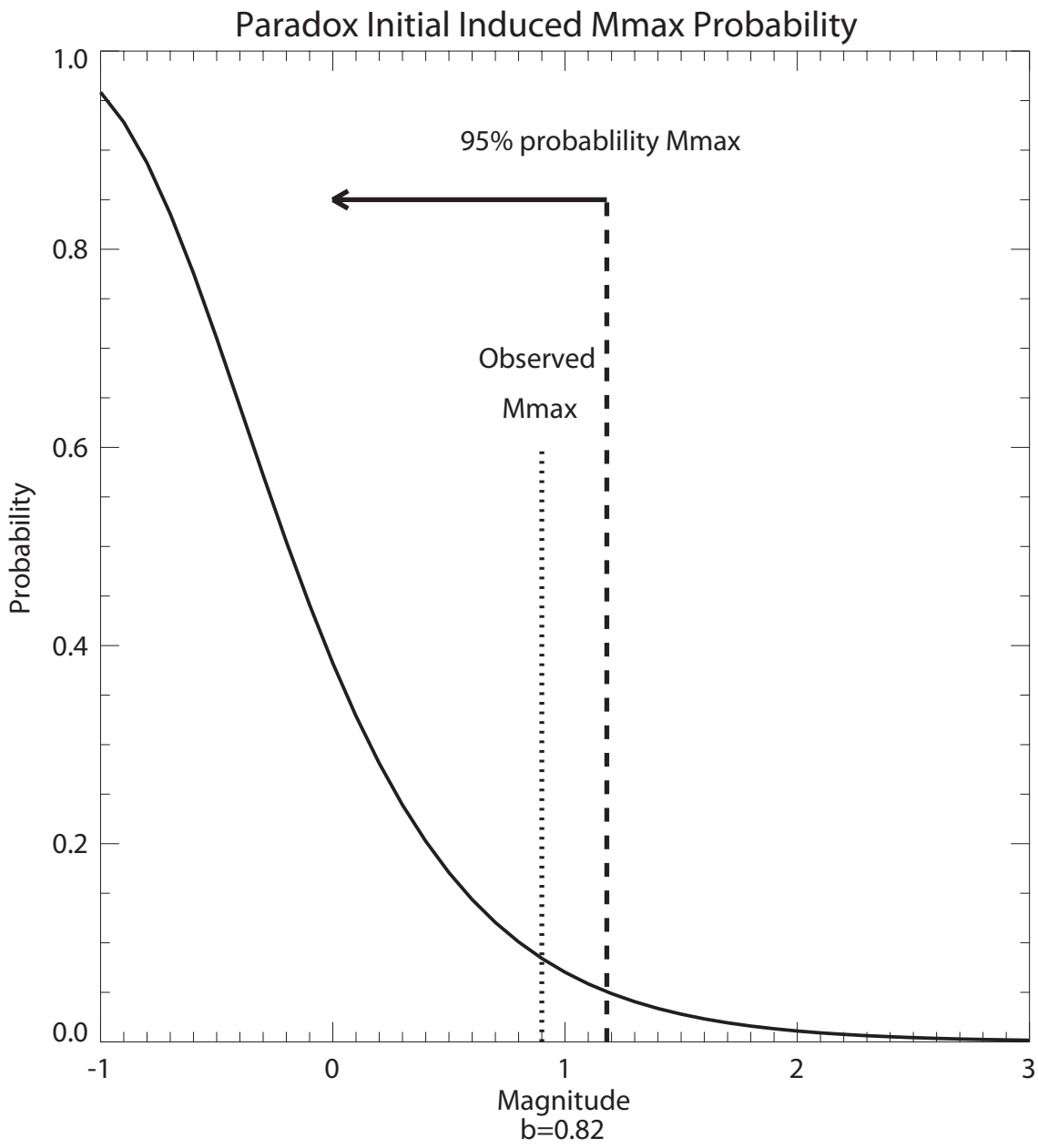

Comparison of Shapiro et al. (2010) predicted Mmax and observed Mmax
For the Paradox Valley 1991 14-day 11,000 m³ Initial Injection Sequence

FIGURE 9

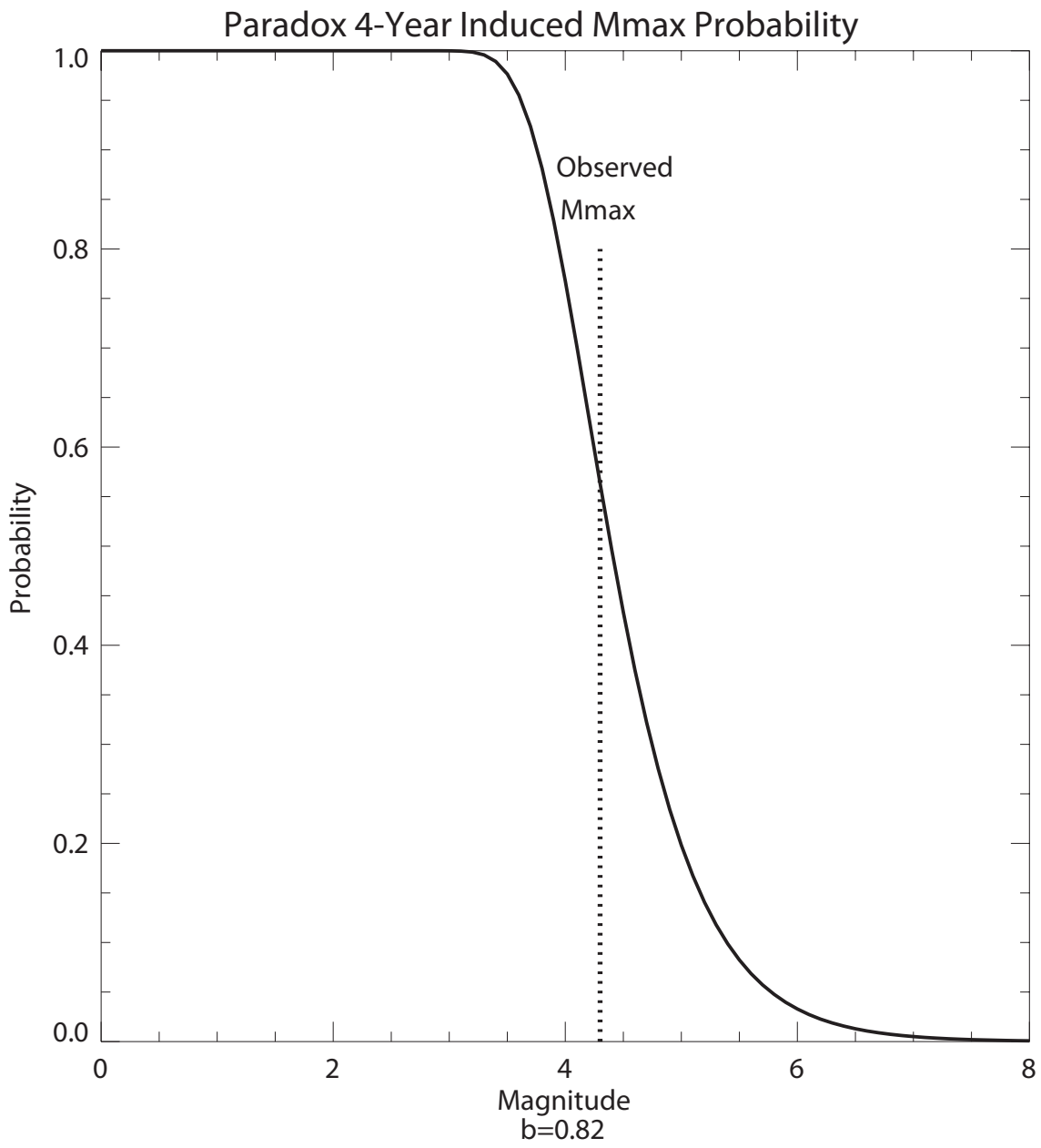

Comparison of Shapiro et al. (2010) predicted Mmax and observed Mmax
For the Paradox Valley 1996-2000 >2,000,000 m³ Injection Sequence

FIGURE 10

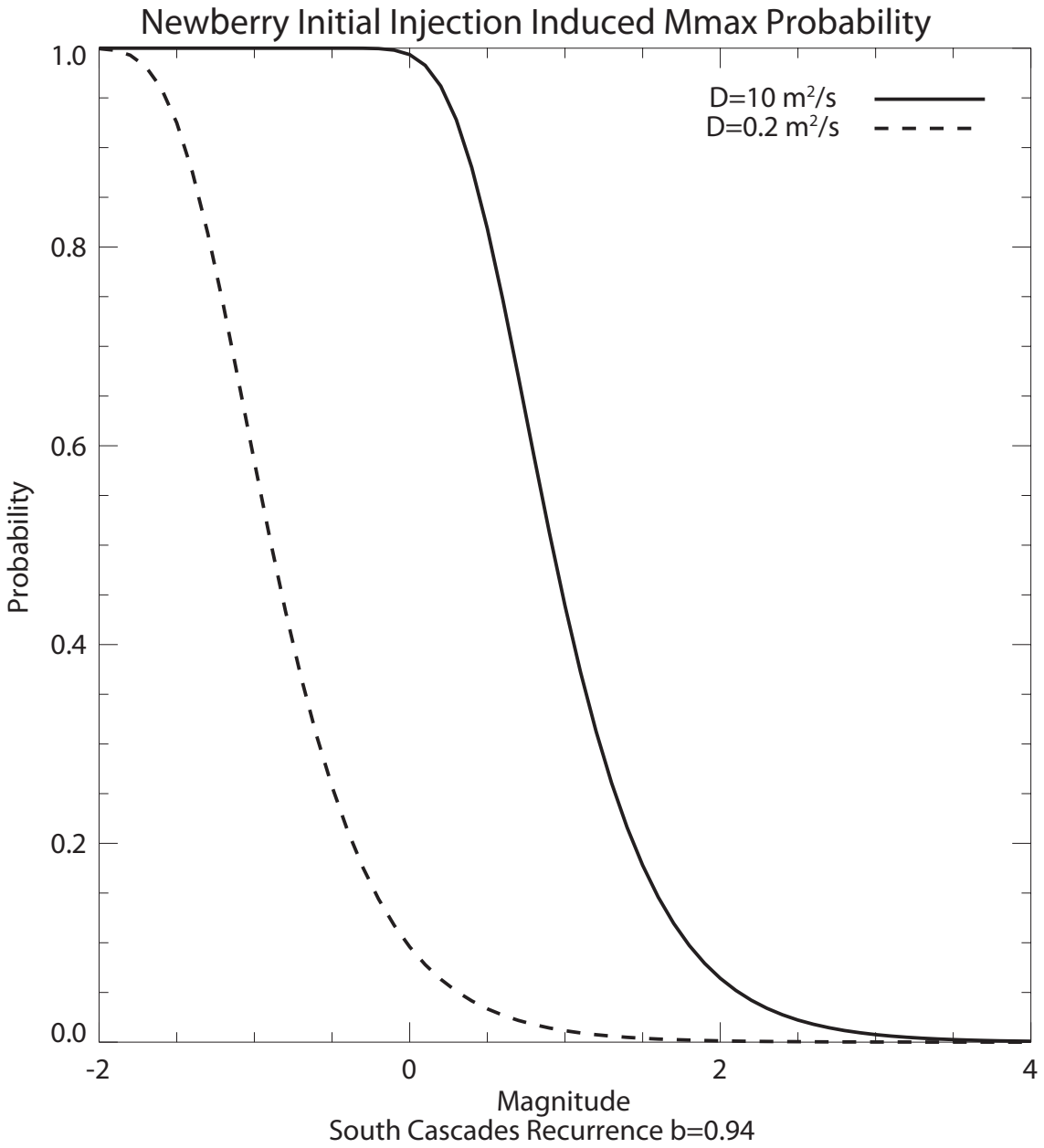

Newberry Induced Mmax Probability with South Cascades Seismicity Rate for b = 0.94

FIGURE 11

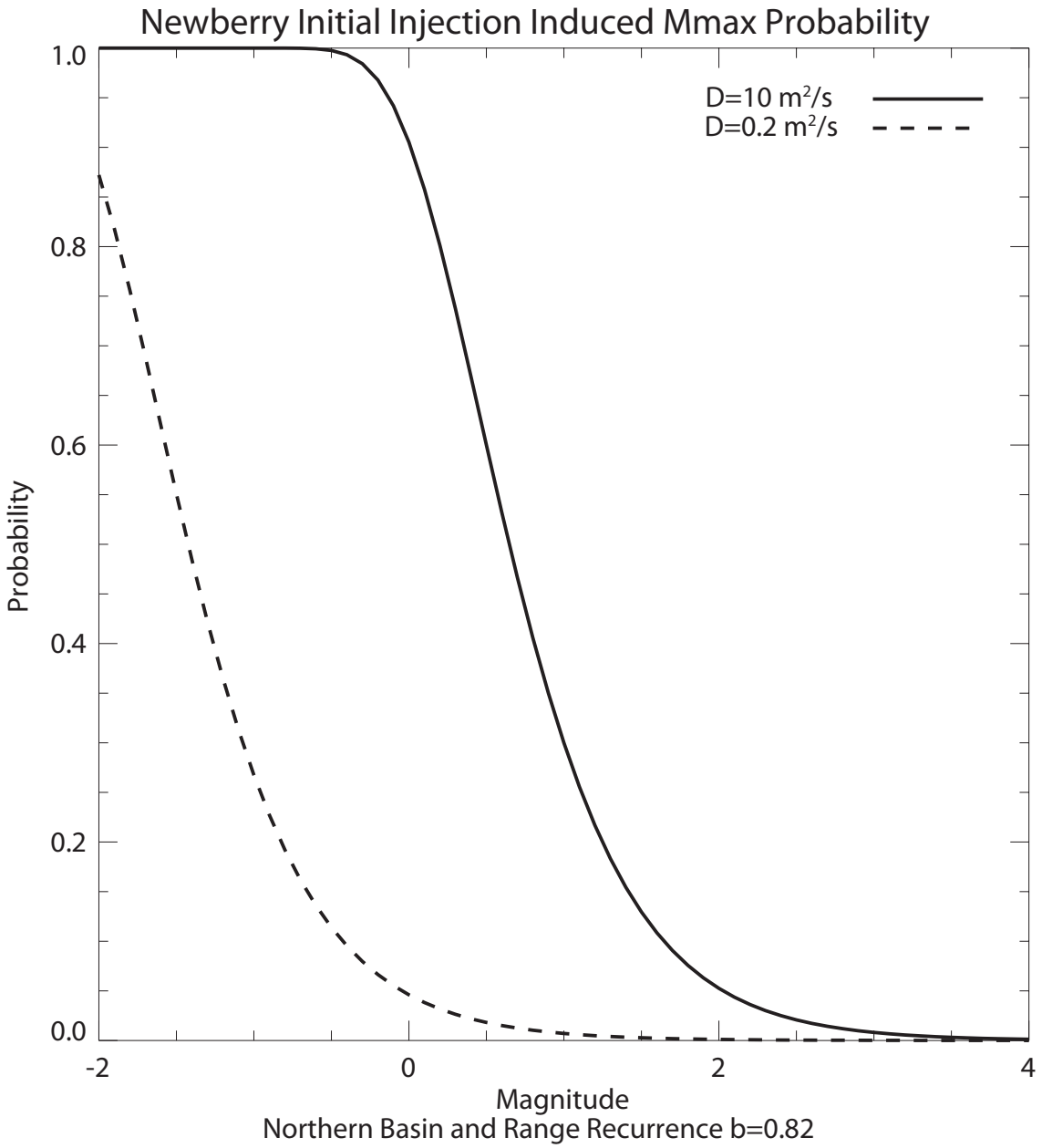

Newberry Induced Mmax Probability with Northern Basin and Range Seismicity Rate for b = 0.82

FIGURE 12